



HAL
open science

StructMap: Elastic Distance Analysis of Electron Microscopy Maps for Studying Conformational Changes

Carlos oscar Sanchez sorzano, Ana lucia Alvarez-Cabrera, Mohsen Kazemi,
Jose maría Carazo, Slavica Jonić

► **To cite this version:**

Carlos oscar Sanchez sorzano, Ana lucia Alvarez-Cabrera, Mohsen Kazemi, Jose maría Carazo, Slavica Jonić. StructMap: Elastic Distance Analysis of Electron Microscopy Maps for Studying Conformational Changes. *Biophysical Journal*, 2016, 110 (8), pp.1753-1765. 10.1016/j.bpj.2016.03.019 . hal-01311676

HAL Id: hal-01311676

<https://hal.sorbonne-universite.fr/hal-01311676>

Submitted on 4 May 2016

HAL is a multi-disciplinary open access archive for the deposit and dissemination of scientific research documents, whether they are published or not. The documents may come from teaching and research institutions in France or abroad, or from public or private research centers.

L'archive ouverte pluridisciplinaire **HAL**, est destinée au dépôt et à la diffusion de documents scientifiques de niveau recherche, publiés ou non, émanant des établissements d'enseignement et de recherche français ou étrangers, des laboratoires publics ou privés.

StructMap: Elastic distance analysis of electron microscopy maps for studying conformational changes

C. O. S. Sorzano¹, A. L. Alvarez-Cabrera¹, M. Kazemi¹, J. M. Carazo¹, and S. Jonić^{2,*}

¹ Biocomputing Unit, Centro Nacional de Biotecnología – CSIC, Campus de Cantoblanco, Darwin 3, 28049 Madrid, Spain.

² IMPMC, Sorbonne Universités - CNRS UMR 7590, UPMC Univ Paris 6, MNHN, IRD UMR 206, 75005 Paris, France.

* Corresponding author (Slavica Jonic, IMPMC-UMR 7590, Université Pierre & Marie Curie, Case courrier 115, 4 Place Jussieu, 75005 Paris, France, Phone : +33 1 44 27 72 05, Fax : +33 1 44 27 37 85, E-mail : Slavica.Jonic@impmc.upmc.fr).

Running title: StructMap method to study conformations

Keywords: Structure, dynamics, macromolecular complexes, electron microscopy, conformational changes

Abstract: Single-particle electron microscopy (EM) has been shown to be very powerful for studying structures and associated conformational changes of macromolecular complexes. In the context of analyzing conformational changes of complexes, distinct EM density maps obtained by image analysis and three-dimensional (3D) reconstruction are usually analyzed in 3D for the interpretation of structural differences. However, graph visualization of these differences based on a quantitative analysis of elastic transformations (deformations) among density maps has not been done yet due to the lack of appropriate methods. Here, we present an approach that allows such visualization. This approach is based on statistical analysis of distances among elastically aligned pairs of EM maps (a map is deformed to fit the other map), and results in visualizing EM maps as points in a lower-dimensional distance space. The distances among points in the new space can be analyzed in terms of clusters or trajectories of points related to potential conformational changes. The results of the method are shown with synthetic and experimental EM maps at different resolutions.

INTRODUCTION

Single-particle analysis (SPA) of two-dimensional (2D) transmission electron microscopy (EM) images of isolated biological macromolecular complexes is routinely used to compute three-dimensional (3D) density maps of a wide range of complexes (*e.g.*, proteins, ribosomes, viruses) (1). In this way, EM information, integrated with a large range of other types of data (*e.g.*, from X-ray crystallography, nuclear magnetic resonance (NMR), modeling, etc.), often provides very valuable information on how these macromolecular complexes perform their function in the cell.

EM density maps are ideally computed from images of complexes having identical conformation and different, uniformly distributed, random orientations. However, quite often, complexes present some degree of flexibility. Methodological extensions of SPA have thus been proposed to analyze flexible complexes (2-11). A classical approach to analyze macromolecular flexibility is to classify a set of particle images into distinct classes composed of particles with similar conformations and, then, to reconstruct an EM density map for each class (2-7). To explain differences between the obtained EM density maps in terms of conformational flexibility, the density maps are analyzed independently as well as with respect to each other (12-16). Multivariate statistical analysis (MSA), introduced to EM for analyzing mixed populations of images in the 1980s (17, 18) and now an integral part of many image analysis approaches and software, allows analyzing and visualization of mixed populations of 2D or 3D data by analyzing principal axes (eigenvectors) of the total data variance. However, to the best of our knowledge, no method currently allows graph visualization of differences among sets of EM density maps based on conformational modeling by elastic transformations (deformations) among maps and a quantitative analysis of these elastic transformations. To fill this gap, we here propose such a method.

The classical, class-based approaches, rest on the assumption that flexibility is discrete, which is not true for a large range of biological systems characterized by continuous flexibility. When flexibility is a continuous process, these class-based approaches may lead to a resolution loss in the density maps coming from the classes because each density map may represent the average conformation of several slightly different conformations that were assigned to the same class. Some recent approaches (8-10) explicitly consider continuous flexibility and perform a multidimensional analysis of particular conformational variables (specific to each approach), which brings all images from the given set of single particle images into a common quantitative reference frame. In this common frame, images are shown as points and distances among points are related to conformational differences among the

corresponding complexes. Such approaches allow analyzing possible trajectories of conformational changes by exploring the regions of the common frame that are most densely populated. The common frame onto which EM data are mapped will be referred to as “distance space” or “map of structures”.

Experimental raw individual 2D images of complexes with continuous flexibility can be seen as spread over some axes described by linear combinations of normal modes, as it has been shown in (8). When density maps are reconstructed from such images grouped, according to conformational similarity, in a few discrete groups along an axis, each of these maps represents the average conformation of slightly different conformations from the same group (8). These density maps can be thus seen as discrete samples of a continuous trajectory. However, the question is whether this trajectory could be extrapolated from its discrete, unordered samples (density maps) obtained by classical, class-based approaches. The approach described here was developed to help with a rough “extrapolation” of the original continuous trajectory from such discrete, unordered samples. This approach is based on a continuous, normal mode analysis (NMA) of a relatively small set of 3D density maps (usually, 3-10), and it could be used as the first step towards a fine extrapolation of the trajectory by methods such as HEMNMA (HEMNMA: Hybrid Electron Microscopy Normal Mode Analysis) that is based on a “continuous” analysis of a large set of 2D images using normal modes of a reference density map (8).

In the proposed approach, each experimental density map is “modeled” by elastic deformation of other density maps from the given set of initially rigid-body aligned maps, in order to compare the maps in terms of their structural and conformational differences. Such modeling is used to evaluate how much one map (target) can be explained by the other map (reference), which is done by computing cross-correlation (normalized between 0 and 1) between the target map and its “model” obtained by deforming the reference map until it best fits the target map (through flexible fitting using normal modes). The unexplained part (what it is left after fitting) is termed “dissimilarity”, and is computed by subtracting the obtained cross-correlation from 1. The dissimilarity measure characterizes the difference (distance) between maps that cannot be explained by flexible fitting. The smaller the dissimilarity, the better the characterization of the deformation between the two maps is in terms of conformational motions described by normal modes. Indeed, normal modes have been shown to be very successful in predicting large-scale low-frequency conformational motions of complexes that were also observed experimentally (19-23). The reference map deformed by flexible fitting is locally rigid-body aligned with the target map before computing the dissimilarity in order to correct for the potential errors in the initial rigid-body alignment that is done without taking into account the deformation. The combined flexible fitting and local rigid-body alignment will be referred to as elastic alignment.

The obtained dissimilarities among the elastically aligned EM density maps are then used to construct a matrix of distances among the density maps. The distance matrix is analyzed using a statistical multivariate analysis method that projects the distances among the density maps onto a lower-dimensional space in which each EM density map is shown as a point. The dimension of the new space is usually one, two, or three, which allows its full visualization. The process of projecting the distance matrix onto a lower-dimensional space is similar to the one used in MSA (17, 18), but the meaning of the distance matrix here is different from the one in MSA. More precisely, the distance matrix in the proposed approach describes pairwise dissimilarities not for pairs of original EM maps, but for pairs of elastically aligned EM maps (basically, after one map was deformed to fit the other one).

In the obtained common quantitative reference frame (map of structures), potential clusters or trajectories of points can be analyzed by the user in terms of conformational changes. The proposed approach will be referred to as “StructMap”, which stands for “Structure Mapping”. The results of StructMap are shown with one set of synthetic EM data and three sets of experimental EM data. The synthetic EM density maps were generated using the EM density map of the closed conformation of the rabbit skeletal muscle type 1 ryanodine receptor (RyR1) complex from Samsó et al (24). The experimental EM density maps comprise the eukaryotic primosome DNA polymerase Pol α – B subunit complex (Pol α – B) from Klinge et al (14), the *E. coli* 70S ribosome complex from Fischer et al (15), and the human 80S ribosomal complex from polysomes from Behrmann et al (25).

MATERIALS AND METHODS

In this section, we describe the methodology that is being proposed as well as the synthesis of the test data set that is used in Experiment 1 of the Results section.

StructMap method

StructMap comprises the following four steps (**Fig. 1A**): 1) preprocessing that consists of 3D-to-3D rigid-body alignment of given EM maps as well as the computation of pseudo-atomic models and the corresponding normal modes of the maps; 2) iterative elastic 3D-to-3D alignment of each pair of EM maps from a given set of EM maps; 3) multivariate analysis of distances among the elastically aligned EM maps; and 4) analysis of the resulting low-dimensional space of distances among EM maps. We here describe each of these steps.

1) Preprocessing - rigid-body alignment of EM maps and computing pseudo-atomic models and corresponding normal modes of EM maps: Before starting the elastic alignment of EM maps in step 2, these maps must be rigid-body aligned as well as possible. More precisely, given two EM density maps, the elastic alignment (step 2) is done by flexible and rigid-body alignments of one density map, referred to as “reference density map”, until it matches the other density map, referred to as “target density map”. However, the rigid-body alignment involved in that step is not global but only local (the initial orientation and position of the deformed reference map with respect to the target map are refined). In this way, the initial rigid-body alignment is corrected at each iteration of the elastic alignment taking into account the deformation estimated at that iteration.

Rigid-body alignment of EM maps is a part of many common data processing workflows. Before using the approach proposed here, the EM maps will thus, most likely, be already globally rigid-body aligned in some way, which was also the case with the experimental EM maps used in this article. Thus, in the preprocessing step of StructMap, in all experiments in this article, given maps were only locally rigid-body aligned, meaning that they were aligned around the orientations and positions in which the maps were available before our work. This rigid-body local alignment was performed using the `xmipp_volume_align` program in Xmipp 3.1. This method was used to refine the alignment of EM maps around the orientation and position in which the maps were available before this work, as aligned by the authors of the maps. However, note that the `xmipp_volume_align` method can optionally be used for a global rigid-body alignment of EM maps, meaning over all rotations and translations, independently of the currently available ones.

In the elastic alignment procedure (step 2), the flexible alignment is based on deforming the reference density map. The density map deformation is realized by displacing a set of 3D Gaussian functions along vectors that are linear combinations of normal modes of the given

density map, where the 3D Gaussian functions are used to model the map densities with the method proposed in (27). More precisely, the reference density map is converted into a collection of 3D Gaussian functions of different amplitudes and positions over the map so that the sum of these Gaussian functions over a voxel approximates the reference-map density at that voxel, with a given mean approximation error over all voxels (27). The 3D Gaussian functions are referred to as “pseudo-atoms”, though their positions do not have to coincide with true atomic positions. The density map representation by pseudo-atoms (PDB-format structure) will be here referred to as “pseudo-atomic model” to distinguish it from a true atomic-resolution structure.

Normal modes of the given EM map are often computed using the elastic network model of the potential energy function of the complex around a minimum energy conformation (8, 19-22, 27, 28), as was the case here. In the elastic network approach, the network is composed of nodes that are 3D point particles connected with springs, where the springs represent harmonic restraints on displacements from the equilibrium conformation (28). Here, the elastic network nodes are 3D Gaussian functions (pseudo-atoms). The elastic network approach based on nodes determined by 3D Gaussian functions was shown to result in computing normal modes that approximate atomic normal modes with high accuracy (8, 27). Additionally, as displacing pseudo-atoms (nodes) along normal modes results in deforming the pseudo-atomic model, such Gaussian-based nodes allow an easy computation of deformed density maps (by summing 3D Gaussian functions) and a comparable resolution of these maps to the resolution of the original, non-deformed density map. The resolution of the pseudo-atomic models (reference and deformed) and the resolution of the deformed density maps can be controlled by controlling the error of pseudo-atomic approximation of the given density map (27). Such deformed density maps are compared with the target density maps in the elastic alignment procedure (step 2) to estimate the deformation.

The user-friendly HEMNMA graphical interface (29) was used here for both computing pseudo-atomic models and normal modes. More precisely, we used a previously developed software for converting EM maps into pseudo-atoms (27) and for NMA (developed by Tama et al (22)), which were also used in our previous work based on normal modes of pseudo-atomic models (8, 27), before being integrated in HEMNMA (29). More details on the use of HEMNMA for these two tasks are given in a separate subsection of this section (see the subsection entitled “Use of HEMNMA for computing pseudo-atomic models and normal modes”).

2) Iterative elastic 3D-to-3D alignment of EM density maps: The proposed method involves elastic 3D-to-3D alignment in the continuous, NMA framework, which was realized by extending and modifying the elastic 3D-to-2D alignment method of (8), available via HEMNMA interface (29). The elastic alignment here means a combined flexible and rigid-body local alignment of one map with the other. The flexible alignment of two maps is performed by deforming one map using normal modes until it fits the other map, and the deformation is realized by displacing pseudo-atoms with a linear combination of normal modes, as in (22, 27). Pseudo-atoms (3D Gaussian functions modeling the original, non-deformed EM map) are displaced, using normal modes, with respect to their location in the original map, meaning that the flexible alignment is local around the conformation given by the original map. However, recall that normal modes describe low-frequency large-scale conformational changes, which means a relatively large range of global deformation amplitudes (several nanometers). The rigid-body alignment of two maps is performed by rotating and translating one map until it fits the other. The elastic alignment procedure

assumes that maps were initially rigid-body aligned (prior to computing pseudo-atoms and normal modes in the preprocessing step) so that it only performs local rigid-body alignment (refinement of current orientations and translations). The transformation of the map by elastic alignment can thus be mainly described as the map deformation because the rigid-body alignment part of transformation will be small for initially rigid-body aligned maps.

The iterative elastic alignment method consists in refining the amplitude of displacement in each normal mode (elastic parameters) as well as the orientation and position (rigid-body parameters) of the reference density map until it matches the target density maps. This is done by minimizing dissimilarity between the two maps, and this dissimilarity (the objective function to be minimized) is here defined as $S=I-CC$, where CC is the cross-correlation between the elastically aligned reference and target density maps. The optimization of the objective function is done with Powell's UOBYQA method that uses a quadratic-approximation local model of the objective function subject to a trust region (30). The UOBYQA method takes into account the curvature of the objective function by constructing interpolant quadratic models. A typical iteration of the algorithm generates a new vector of variables (new point) by minimizing the quadratic model. The objective function is then evaluated at the new point and one of the interpolation points is replaced by this new point (30).

The trust-region radius is related to the length of steps that are used in the objective function optimization (30). Its meaning here is the norm of the vector of normal-mode displacement-amplitude differences between points at which the objective function is evaluated, where points are vectors of the displacement (deformation) amplitudes and the vector dimension is the dimension of the search space given by the number of normal modes. The trust-region is a ball around the best point found currently, with the radius given by the trust-region radius. As the deformation amplitudes, the trust-region radius has no physical units, as the NMA software used here computes the coordinates of normal mode vectors in angstroms while it displaces pseudo-atoms using normal-mode displacement amplitudes without units. Trust-region-based approaches are known to be more robust to noise thanks to the regularization effect of minimizing objective-function models (usually quadratic) around current iterates over regions of controlled size. The trust-region radius is adapted iteratively to optimize the trust-region size. Actually, the UOBYQA method uses two radii; one (ρ) is not allowed to increase because this would necessitate expensive decrease later; the other (Δ) satisfies $\Delta \geq \rho$ and allows the length of steps to exceed ρ , which improves the efficiency of the algorithm (30). The method requires setting the initial vector of displacement amplitudes (initial point), the maximum number of iterations, the initial and final values of the trust region radius ρ , and sets the initial value of Δ to be equal to the initial value of ρ .

The developed 3D-to-3D elastic alignment software uses an implementation of the UOBYQA method from CONDOR libraries (31). The 3D-to-3D elastic alignment method is available in Xmipp (32-34) (version 3.1) as a program under the name *xmipp_nma_alignment_vol*. This program aligns a reference pseudo-atomic model (obtained from a reference EM density map) with a set of target EM density maps, and requires that all density maps have the same size (in voxels) and the same voxel size (in angstroms). For each target EM density map, the reference pseudo-atomic model is deformed and its orientation and position refined so that the corresponding density map (after the displaced pseudo-atoms are converted into the density map format) best matches the target EM density map.

In the proposed approach, the initial displacement amplitudes are equal to zero, meaning that the non-deformed reference pseudo-atomic model is used to initialize the first iteration. In each UOBYQA iteration (**Fig. 1B**), the pseudo-atomic model is displaced with the new guess of the normal-mode displacement amplitudes (new point) obtained by minimizing the quadratic model, and the modified pseudo-atomic coordinates are converted into a density map. Then, this density map is locally rigid-body aligned with the target density map. The rigid-body alignment is done with a fast rotational matching method that maximizes the cross-correlation between two density maps (26), and the objective function S is evaluated after this alignment. The local model of the objective function is then reconstructed around the new point, and a new iteration is started by finding the minimum of the current local model of the objective function and moving the current vector of deformation amplitudes (current point) to this minimum. The iterations are repeated until reaching the final value of the trust-region radius ρ or the maximum number of iterations. All experiments in this article were performed using the initial and final values of the trust-region radius ρ and the maximum number of iterations of 250, 50, and 10,000, respectively. Within a similar objective-function optimization procedure (in HEMNMA), these values have been shown to produce good results with several complexes of different amplitudes of conformational changes (70S ribosome, Pol α – B complex, and Tomato Bushy Stunt Virus) (8). They are set as default values in *xmipp_nma_alignment_vol*. The use of trust-region radii improves the optimization convergence, by improving robustness to noise, but UOBYQA does not guarantee reaching the global optimum. Though reaching the global optimum cannot be guaranteed, the method provides rather good solutions, as shown in this article.

The main difference between the objective-function optimization in the elastic alignment procedure in HEMNMA and in StructMap is a different nature of target data (2D images in HEMNMA vs 3D density maps in StructMap). As the reference data are in both cases 3D density maps, HEMNMA is based on elastic 2D-to-3D data alignment, whereas StructMap is based on elastic 3D-to-3D data alignment. This means that the elastic alignment procedure in HEMNMA requires computing 2D projections of a 3D density map (to perform its matching with target images), which is not the case of StructMap. Note here that this comparison is only done regarding technical details of the two elastic alignment procedures, and not regarding the results that the entire StructMap and HEMNMA methodologies can produce. Actually, StructMap is not meant to replace HEMNMA because the two methodologies are complementary and can be combined, as shown in Results (Experiment 2) and discussed further in Discussion.

3) Multivariate distance analysis: The optimized value of the dissimilarity measure, S , obtained for each aligned pair of EM density maps is used to construct an N -by- N symmetrical distance matrix D , where N is the number of given EM maps. As the alignment of the i -th EM map, V_i , with respect to the j -th EM map, V_j , is done through elastic geometric transformations of V_i until it matches V_j , this alignment will result in dissimilarity S_{ij} that will generally be different from S_{ji} , representing the dissimilarity of V_j aligned with respect to V_i . Thus, we set the ij -th and ji -th elements of the distance matrix D (D_{ij} and D_{ji} , respectively) to be the average between S_{ij} and S_{ji} (i.e., $D_{ij}=D_{ji}=(S_{ij}+S_{ji})/2$). Note that the differences between S_{ij} and S_{ji} are usually small (a strong asymmetry of the distance matrix would indicate that the underlying matching of one volume into the other is ill-defined, which was not observed here). We set $D_{ii}=0$ since there is no distance from an EM density map to itself.

To perform multivariate analysis of the distance matrix, we use a non-metric multidimensional scaling method (35) that is available in MATLAB (MATLAB and Statistics

Toolbox Release 2011b, The MathWorks, Inc., Natick, Massachusetts, United States) under the name *mdscale*. The method returns N points in p dimensions, where the number of dimensions p ($p \leq N$) is an input parameter (in normal practice, $p=1$, $p=2$ or, at most, $p=3$), such that the Euclidean distances between the obtained points approximate a monotonic transformation of distances in the distance matrix. The *mdscale* method optimizes the so-called Kruskal's normalized stress (35) function that measures the degree of correspondence between the input distance matrix and the output points. The points are plotted in a p -dimensional distance space (map of structures). In this article, results of the *mdscale* method are deterministic as the method was used with no randomness option.

4) Analysis of the map of structures: The pattern that the points make in the new, p -dimensional space, together with their relative distances, can be used to identify clusters of points that correspond to similar EM maps. In some cases, the disposition of points in the p -dimensional space can also be used to explore potential sequences of conformational changes that we will then refer to as “trajectories of points”.

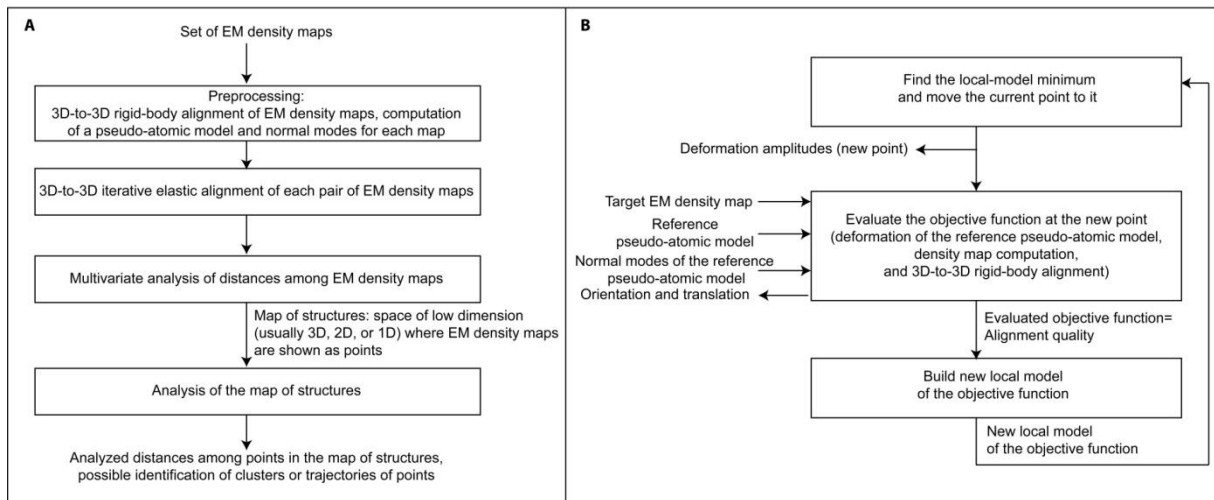


Figure 1: Flowchart of the proposed StructMap method (A) and the iterative elastic 3D-to-3D alignment step between any two EM density maps (B). The measure of dissimilarity between two finally aligned EM density maps is taken as the distance between the two maps. The distances among all pairs of EM maps are used to construct a distance matrix that is then analyzed with a multivariate analysis method, so as to project all EM maps onto a common distance space (map of structures), in which each EM map is represented as a point. Points may then be analyzed in terms of their positions and mutual distances to potentially identify clusters or trajectories of points.

Data generation for the experiment with synthetic EM maps

For one of the experiments performed with the proposed method, we discretized two distinct synthetic trajectories of continuous conformational changes of the same complex. The two synthesized trajectories are completely fictional and may not exist or coexist in the experimental case. They were synthesized by displacing the EM map of the closed conformation of RyR1 (from Samso et al (24)) using two different normal modes from the same set of normal modes. The two normal modes used for the displacement were selected to produce opening-closing movements of RyR1. The displacement in one of the two modes (mode 8) produces symmetrical conformational changes that correspond to those usually reported in the literature. By “symmetrical changes” we mean that the object remains symmetrical after the displacement using normal modes. The displacement in the other mode (mode 9), in turn, produces asymmetrical conformational changes. By “asymmetrical changes” we mean that the object becomes asymmetrical after the displacement using normal modes. To the best of our knowledge, those asymmetrical changes have not been previously

reported. The synthesis of this test data set is fully described in this section. The results of the experiment with this data set are given in the Results section (Experiment 1).

We used the EM density map of the closed conformation of RyR1 deposited at the EMDB with code EMD-1606 (24) (resolution: 10.2 Å; size: 180 × 180 × 180 voxels; voxel size: 2.8 Å × 2.8 Å × 2.8 Å). The pseudo-atomic model of the EM density map and its normal modes 8 and 9 were used to compute 8 additional pseudo-atomic models. The density maps obtained from the 9 pseudo-atomic models were projected to obtain 500 randomly oriented projections for each density map. The projections had a uniform angular distribution, the size of 128×128 pixels, and the pixel size of 3.94 Å × 3.94 Å. Note here that the projection resolution is lower than the resolution that could be obtained by projecting the obtained density maps onto the image planes whose size is given by the original density map size (i.e., image size of 180 × 180 pixels and the pixel size of 2.8 Å × 2.8 Å), which was chosen to “simulate” a real experiment as, in practice, the object’s 2D projection images are collected at a limited resolution, due to image formation and detection limitations. Each projection was modified by adding simulated experimental noise and contrast transfer function (CTF). The CTF and noise were simulated for a 200 kV microscope with a spherical aberration of 2 mm, defocus of 1 μm and signal-to-noise ratio of 0.2, using the method of Velazquez-Muriel et al (36). Finally, each of the 9 sets of simulated images was used to compute the corresponding 3D reconstruction (**Fig. 2A-E**). Note here that resolution of the reconstructed density maps is low (around 20 Å), as a relatively small number (500) of noisy and CTF-affected images was used for the reconstruction.

The reconstructed density map referred to as 1 corresponds to the non-displaced initial pseudo-atomic model (i.e., zero displacement amplitudes in all modes) (**Fig. 2A**). Four of other reconstructed density maps, referred to as 2, 3, 4, and 5 (**Fig. 2B-C**), correspond to the displacement of the initial pseudo-atomic model in mode 8 using the displacement amplitude of 300, 500, -300, and -500 (no units), respectively, and zero displacement amplitudes in other modes. Four additional reconstructed density maps, referred to as 6, 7, 8, and 9 (**Fig. 2D-E**), correspond to the displacement of the initial pseudo-atomic model in mode 9 using the displacement amplitude of 300, 500, -300, and -500 (no units), respectively, and zero displacement amplitudes in other modes.

Figure 2B-C shows that the sequences of discrete states 3-2-1-4-5 and 5-4-1-2-3 describe symmetrical opening and closing of the complex, respectively, whereas **Figure 2D-E** shows that sequence 7-6-1-8-9 (or 9-8-1-6-7) describes asymmetrical opening or closing of the complex (one side of the complex opens while the other side closes).

Use of HEMNMA for computing pseudo-atomic models and normal modes

As mentioned earlier in this section, the pseudo-atomic models and their normal modes were computed using the HEMNMA graphical interface (29). In this subsection, we give more details on the HEMNMA parameter settings used for this purpose.

The HEMNMA graphical interface (29) allows using a 3D binary mask and adjusting the desired EM-map approximation error and the standard deviation of Gaussian functions (for computing pseudo-atomic models), the interaction cut-off distance between pseudo-atoms (for computing normal modes), the number of lowest-frequency normal modes to be analyzed in terms of their collectivity and the collectivity threshold (for selecting the modes that will be used in the further analysis that is here the elastic alignment of EM density maps). The 3D binary mask can be used to assure that some parts of the EM density map are not represented

by Gaussian functions (e.g., a noisy background of the complex). Here, the 3D binary mask was obtained by a combination of EM-map thresholding and several morphological operations. The desired error of the EM-map representation by Gaussian functions determines the end of the iterative process by which Gaussian functions are added to the pseudo-atomic representation and, here, it was set to a value of 5% that usually results in good representations (29). The Gaussian-function standard deviation was adjusted to a value between 1 and 2 voxels, as typically done to better optimize the EM-map approximation error (29). The elastic network model for the computation of normal modes has the interaction cut-off distance parameter that determines the distance between the pseudo-atoms above which they do not interact, and its value is usually adjusted between 10 Å and 30 Å according to the size of the complex (in voxels) (8, 22). Here, the interaction cut-off distance parameter was set to 10 Å for Pol α – B, 25 Å for 70S and 80S, and 30 Å for RyR1. It has been shown that highly collective low-frequency modes are relevant to functional conformational changes (19, 20) and that such changes can usually be described by a few modes among the first (lowest-frequency) twenty to fifty pseudo-atomic normal modes (8, 22). The collectivity degree (37) measures the collectivity of motions in a normal mode by counting the number of pseudo-atoms affected by the mode. The collectivity degree approaches 1 for maximally collective motions and 0 for localized motions (37). Here, the collectivity degree was computed and analyzed for the first twenty normal modes in the case of lower-resolution density maps (synthetic maps of RyR1 and experimental maps of Pol α – B) while the first thirty normal modes were analyzed in terms of collectivity in the case of higher-resolution density maps (experimental maps of 70S and 80S). The modes collectivity threshold determines a subset of the total set of normal modes that will be used for a further analysis. The collectivity threshold of 0.15 was used here, which means that only the modes with the collectivity degree above 0.15 were used for the elastic alignment of EM density maps. The collectivity threshold of 0.15 has been shown to successfully reject poorly collective modes that are very likely unrelated to functional conformational changes (8, 29). The six lowest-frequency modes were not used either, as they are related to rigid-body movements (8, 22, 29).

RESULTS

In this section, we show the performance of the StructMap method with synthetic and experimental EM density maps. The most important information gained by using StructMap are the graphical and numerical distance-space results i.e. the overall, graphical view of differences (distances) among a set of elastically aligned density maps (represented by points in the distance space) as well as all pairwise distances among these maps. In the distance space, some pairs of points are connected by lines to help discuss distances among points and a potential disposition (configuration) of points in clusters or trajectories in the distance space. In the experiments with experimental EM maps (Experiments 2-4), lines are drawn to connect points representing subsequent states according to the previously published work in which these maps were obtained, which was done to visualize the patterns that these previously published results (sequences) make in the distance spaces obtained in this work. In the experiment with synthetic EM maps (Experiment 1), lines are drawn to connect points following their ground-truth order (i.e. the synthesized sequence of states 5-4-1-2-3 and 9-8-1-6-7), which was done to visualize the pattern that this ground-truth order makes in the obtained distance space. The summary of all pairwise point distances obtained by analyzing the sets with more than three EM maps is given in Supporting Material (**Tables S1-S3**).

Figures in this section also show rigid-body aligned density maps (from the preprocessing step) that are complemented with arrows indicating the movements mainly contributing to the elastic transformation (deformation) between maps, and the arrow scale shows the distance

between maps in the distance space. This is additional information gained by using StructMap.

Experiment 1: Analysis of synthetic EM density maps

Here, we present the results of StructMap using the synthetic data set that was described in the Materials and Methods section. The goal of the experiment was to analyze the pattern created by the synthetic EM density maps in the resulting map of structures, in order to see how the synthesized conformational trajectories look like in this map (e.g., as two distinct trajectories or not). Recall that the synthesized conformational trajectories are completely imaginary, which means that the results presented here should not be interpreted in terms of experimental RyR1 conformational changes. A pseudo-atomic model and its 20 normal modes were computed for each given synthetic density map. Then, each density map (via its pseudo-atomic model) was elastically aligned with all other density maps and the obtained 9-by-9 distance matrix was projected onto a space of three, two, and one dimensions (**Figs. 2F and 3A-B**, respectively).

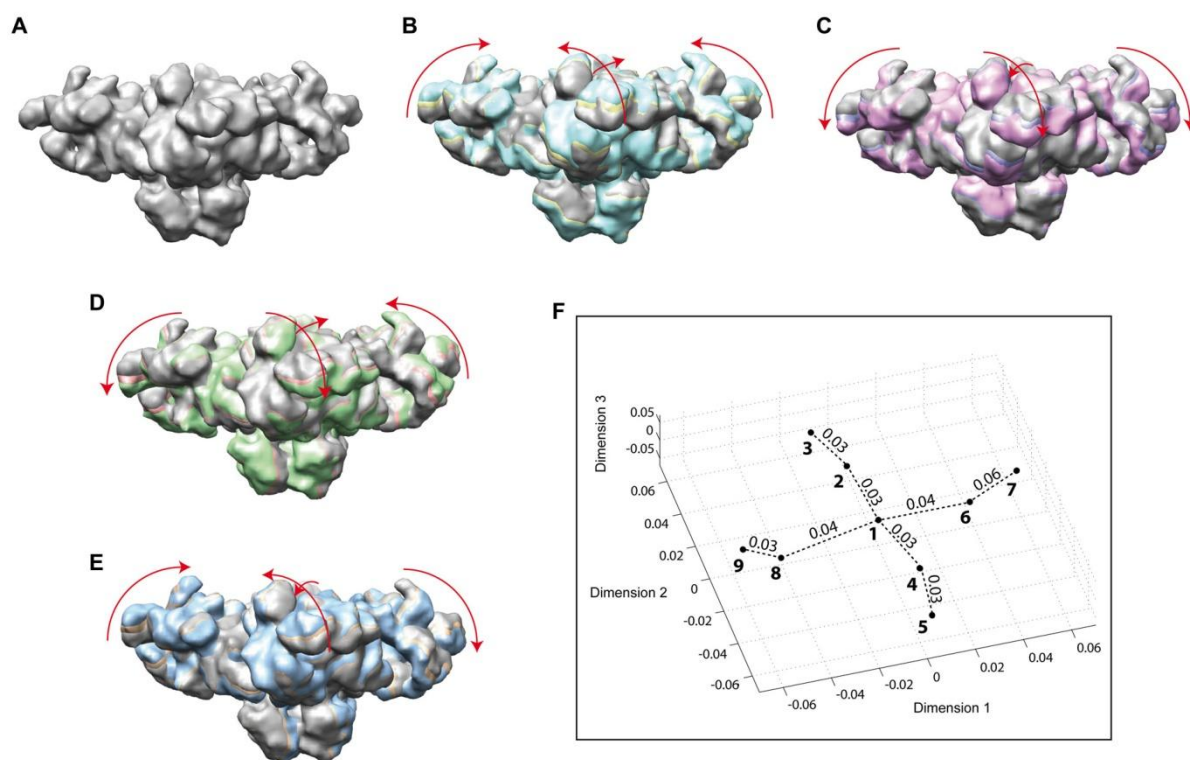


Figure 2: Synthetic RyR1 data experiment using synthetic density maps representing symmetrical (B-C) and asymmetrical (D-E) structural changes of the complex (A). (A) Synthetic density map 1. (B) Map 1 (grey) overlapped with maps 2 (yellow) and 3 (cyan). (C) Map 1 (grey) overlapped with maps 4 (violet) and 5 (magenta). (D) Map 1 (grey) overlapped with maps 6 (pink) and 7 (green). (E) Map 1 (grey) overlapped with maps 8 (brown) and 9 (blue). (F) Projection of density maps onto a 3D distance space. In A-E, all density maps are viewed from the same viewing direction. In each of panels A-E, arrows show main directions of deformation of map 1 (grey) when fitting the other two maps (overlapped), and the arrow scale shows the largest distance among these three maps after the deformation according to Table S1. In F, the density maps are marked with their indexes and circles, and the length of each dotted line segment is the distance between two conformations that is shown above the segment in arbitrary units. See also **Figure 3**.

In the 3D distance space, one can note a two-trajectory configuration of points 1-9 that correspond to synthetic density maps 1-9, respectively (**Fig. 2F**). This two-trajectory configuration is visually emphasized by connecting points following their ground-truth order (i.e. 5-4-1-2-3 and 9-8-1-6-7). The different distances among neighboring points on the two

trajectories mean that the same deformation amplitude has a different impact on the two types of deformations, from the point of view of the mapped dissimilarity measure. More precisely, the larger distances on trajectory 9-8-1-6-7 than on trajectory 5-4-1-2-3 suggest that the same deformation amplitude has a larger impact on the asymmetrical deformation than on the symmetrical deformation. All pairwise point distances obtained in this experiment are summarized in Table S1.

As 2D and 1D maps of structures could also be useful in practice, especially when analyzing a small number of EM maps, we projected the same set of synthetic density maps onto these two spaces as well. The results of projecting density maps onto a 2D distance space are consistent with those obtained by projecting the same density maps onto a 3D distance space (**Fig. 3A**). Regarding the projection of the same density maps onto a 1D distance space, there is a non surprising loss of information about the two-trajectory configuration (**Fig. 3B**); however, the 1D distance mapping still allows sorting out similar and dissimilar density maps. For instance, **Figure 3B** clearly shows that density maps 1, 2, and 4 are the most similar ones, whereas maps 7 and 9 are the most dissimilar. Thus, 1D distance mapping may still be useful when analyzing a small number of EM density maps (*e.g.*, 3-4 density maps), as in the case shown in Experiment 2.

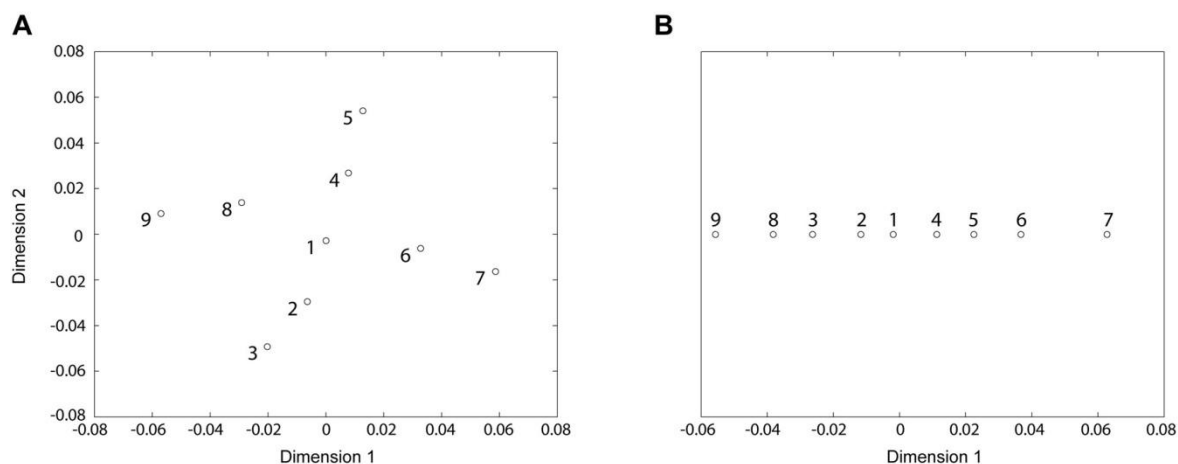


Figure 3: Projection of synthetic RyR1 density maps onto a distance space of a lower dimension than 3. (A) 2D distance space. (B) 1D distance space. The density maps are marked with their indexes and circles. See also **Figure 2**.

Experiment 2: EM density maps of Pol α – B

In this experiment, we used three EM density maps of Pol α – B from Klinge et al (14). They correspond to different states of bending of the flexible linker between two lobes of the complex. The EM density maps have the size of $64 \times 64 \times 64$ voxels, the voxel size of $3.8 \text{ \AA} \times 3.8 \text{ \AA} \times 3.8 \text{ \AA}$, and the resolution between 23 \AA and 25 \AA . They are referenced by indexes 1, 2, and 3, as obtained from the authors (14). A pseudo-atomic model and its 20 normal modes were first computed for each EM density map. Then, each density map (via its pseudo-atomic model) was elastically aligned with all other density maps, and the obtained 3-by-3 distance matrix was projected onto a 1D distance space (**Fig. 4A**).

The 1D distance mapping results (**Fig. 4A**) show that EM density map 1 is almost equally distant from the other two EM density maps (the distance of map 1 to the other two maps is around 0.1). Thus, this sequence could be interpreted as a movement around conformation 1, in the order 3-1-2 or 2-1-3 (**Fig. 4B**). EM maps in the order 3-1-2 correspond to the unbending of the complex from conformation 3 to conformation 2 (**Fig. 4B-C**). These results are

coherent with previously published results (Fig. 6 of Klinge et al (14)) but, contrary to the previous study, they are here based on a quantitative distance analysis.

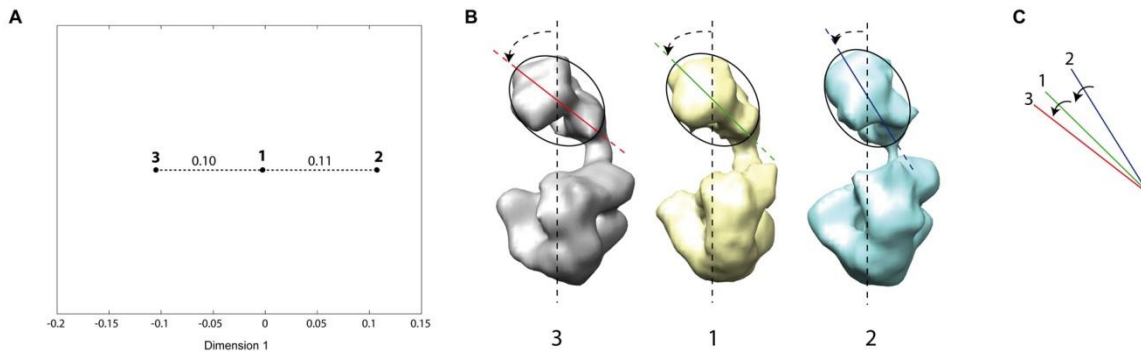


Figure 4: Projection of three EM density maps of DNA polymerase Pol α - B complex onto a 1D distance space. (A) 1D distance space (EM maps are marked with circles and the length of each dotted line segment is the distance between two EM maps that is shown above the segment in arbitrary units). (B) Ordered rigid-body aligned EM density maps (3-1-2) according to their disposition in the distance space shown in A, together with dashed arrows showing different degrees of bending of the complex i.e. rotation of the upper lobe towards the lower lobe (the elastic transformation among these maps is mainly described by the bending movement). (C) Upper-lobe axis of overlapped maps 1-3, shown with the same color as the color of the upper-lobe axis in B (red: map 3; green: map 1; blue: map 2), together with solid arrows showing the deformation direction (the rotation of the upper lobe of map 2 towards map 1 and the rotation of the upper lobe of map 1 towards map 3). In C, the arrows do not show the amount of deformation but they show (by the arrow scale) the distance between maps in the map pairs (1,2) and (1,3) after the deformation according to panel A. Note that the vertical lines shown in B and C are not the same but they are parallel to each other.

These results could be used in combination with HEMNMA to explore conformational changes of Pol α - B at a finer level of details, by a continuous analysis of 2D images using normal modes of a reference density map, as was done in (8). In this context, the results of StructMap could be used to select the reference density map for analyzing images by HEMNMA. Actually, in (8), 12000 Pol α - B single-particle images (used for computing maps 1-3) were analyzed using HEMNMA and map 3 was used as the reference map. The reference map was chosen to be map 3 because this map was obtained from the most populated class of images (maps 3, 1, and 2 come from classes with 42%, 30%, and 28% of the total number of images, respectively (14)). Though map 3 was reconstructed from the largest number of images, or exactly because of that, it is tempting to think that some heterogeneity could have been incorporated in that map. The fact that it is one of the two end points in the distance map (**Fig. 4A**) could support this hypothesis, meaning that some other conformations could exist even further to the left from map 3 in the distance map but they could not be identified (they were somehow hidden) because of splitting images in only three classes. Thus, the results of StructMap (distance map, **Fig. 4A**) show that it would be interesting to use map 3 for the images analysis with HEMNMA to identify conformations that could not be identified by splitting images in only three classes (e.g., those at the left side of map 3 in the distance map), which was actually done in (8). The second end point in the distance map, map 2, would be less interesting to use for the continuous analysis of images (as the reference map for HEMNMA) because it lacks some mass at the level of the linker between the lobes, which was explained by a strong heterogeneity of conformations in the corresponding class of images (14).

Experiment 3: EM density maps of *E. coli* 70S-fMetVal-tRNAVal-tRNA^{fMet} complex

The EM density maps of different pre- and post-translocational states of *E. coli* 70S complex published by Fischer et al (15) were downloaded from EMDB database. Among them, we

have analyzed those that had the same size ($128 \times 128 \times 128$ voxels), the same voxel size ($2.8 \text{ \AA} \times 2.8 \text{ \AA} \times 2.8 \text{ \AA}$), and that contained the entire 70S complex. The analyzed data set contained seven EM density maps of resolution between 12 \AA and 20 \AA (15). These EM maps correspond to the pre-translocational states pre2 to pre5 (EMD-1717 to EMD-1720, respectively) and the post-translocational states post1 to post3 (EMD-1721 to EMD-1723, respectively). A pseudo-atomic model and its 30 normal modes were computed for each EM density map, each density map (via its pseudo-atomic model) was elastically aligned with all other density maps, and the resulting 7-by-7 distance matrix was projected onto a 3D distance space (**Fig. 5A**).

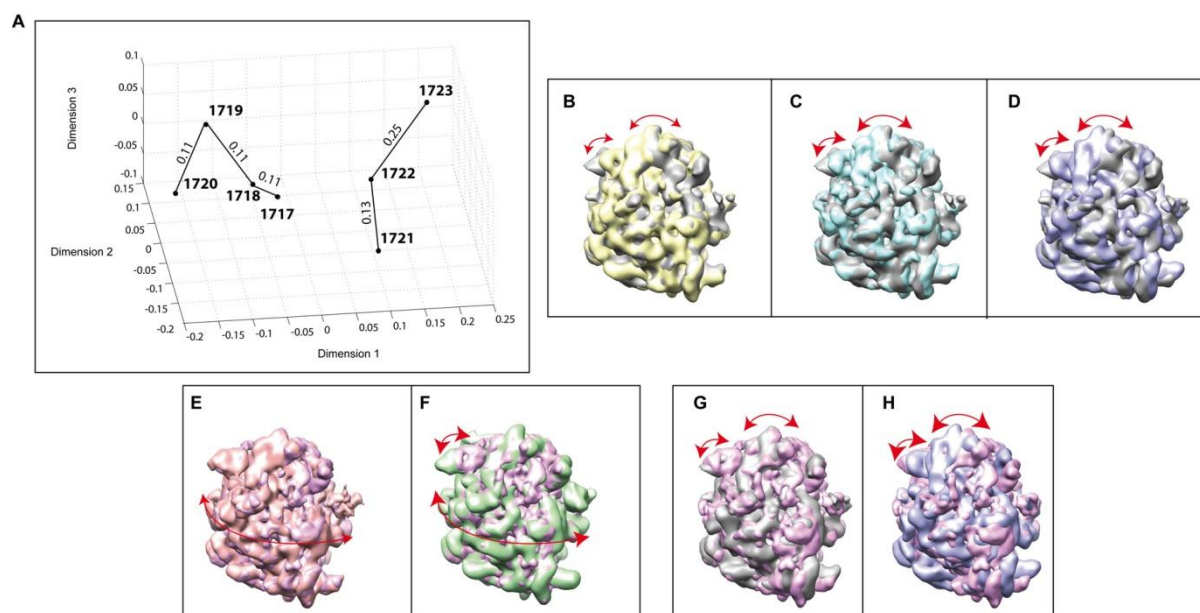


Figure 5: Projection of seven EM density maps of 70S ribosome (EMD-1717 to EMD-1723) onto a 3D distance space. (A) 3D distance space. (B-H) Overlap of rigid-body aligned EM density maps, with the same view for all overlapped maps. (B) 1718 vs 1717 (gray). (C) 1719 vs 1717 (gray). (D) 1720 vs 1717 (gray). (E) 1722 vs 1721 (magenta). (F) 1723 vs 1721 (magenta). (G) 1717 vs 1721 (magenta). (H) 1720 vs 1721 (magenta). In A, the EM maps are marked with circles and the corresponding EMD entry codes. Straight lines are used to connect subsequent states, according to the proposal by Fischer et al (15), and the length of each line segment is the distance between two maps that is shown above the segment in arbitrary units. In each of panels B-H, arrows show the movements that mainly contribute to the elastic transformation (deformation) between two overlapped maps, and the arrow scale shows the distance between these maps in the distance space. Bi-directional arrows were used to recall that StructMap computes the elastic transformation between two maps in both directions. Note that the arrow scale shows dissimilarity between maps after the deformation but the amount of deformation (movement amount) is not represented by arrows. However, note that the type of movement is represented by arrows (i.e., rotation of 30S with respect to 50S and L1 stalk motion in B-D and G-H, rolling/unrolling of the complex in E, and rolling/unrolling of the complex and L1 stalk motion in F).

The 3D map of structures and pairwise map distances (**Fig. 5A**, **Table S2**) show that most distances among maps 1717-1720 (four distances of 0.11, one distance of 0.2, and one distance of 0.21 (arbitrary units)) are smaller than distances of maps 1717-1720 to maps 1721-1723 (three distances of 0.2 and nine distances greater or equal to 0.25 (arbitrary units)). This means that maps 1717-1720 correspond to similar conformational states as well as that these states are generally less different with respect to each other than with respect to states 1721-1723, which is also visible when the maps are overlapped. For instance, the orientation of the 30S subunit is generally more similar between maps 1717-1720 (**Fig. 5B-D**) than is the 30S orientation between these maps and maps 1721-1723 (**Fig. 5G-H**). This is consistent with the findings of Fischer et al (15), indicating that maps 1717-1720 correspond to similar, pre-translocational states, whereas maps 1721-1723 correspond to similar, post-translocational

states. Our results complement the results of Fischer et al (15) by providing a quantitative analysis of the conformational differences. For instance, the results (**Fig. 5A, Table S2**) additionally show that maps 1721 and 1722 are more similar (the distance of 0.13) than maps 1722 and 1723 (the distance of 0.25) or maps 1721 and 1723 (the distance of 0.25), which is also visible in **Figure 5E-F**.

Experiment 4: EM density maps of native human 80S ribosomal complex from polysomes

In this experiment, we used eleven EM density maps of native human 80S ribosomal complexes from polysomes, deposited in EMDB by Behrmann et al (25). They correspond to states along the elongation cycle of 80S (25). In the clockwise direction along the elongation cycle shown in Figure 1 from Behrmann et al (25), the EM density maps correspond to the following states: classical iPRE state (EMD-2907), classical-1 PRE state (EMD-2909), PRE* state (EMD-2906), rotated-1 PRE state (EMD-2904), rotated-2 PRE state (EMD-2905), POST-i3 state (EMD-2903), POST-i2 state (EMD-2902), POST state (EMD-2875), pre-recycling state (EMD-2910), post-decoding/post-hydrolysis state (EMD-2908), and post-decoding/post-dissociation state (EMD-2911). Note that the density maps of translocation and decoding-sampling/-recognition complexes were not used in our experiment, as these complexes were not observed experimentally in the original work (25). The density map EMD-2875 has the size of $400 \times 400 \times 400$ voxels, the voxel size of $0.945 \text{ \AA} \times 0.945 \text{ \AA} \times 0.945 \text{ \AA}$, and the resolution of 3.5 \AA according to the $FSC_{0.143}$ resolution criterion (25). All other EM density maps have the size of $200 \times 200 \times 200$ voxels, the voxel size of $1.89 \text{ \AA} \times 1.89 \text{ \AA} \times 1.89 \text{ \AA}$, and their resolution is between 5 \AA and 10 \AA according to the $FSC_{0.5}$ resolution criterion (25). We thus resized map EMD-2875 so that it has the same number of voxels and the voxel size as the other EM density maps, which is required by StructMap (see Materials and Methods). A pseudo-atomic model and its 30 normal modes were computed for each density map, each density map (via its pseudo-atomic model) was elastically aligned with all other density maps, and the obtained 11-by-11 distance matrix was projected onto a 3D distance space (**Fig. 6A**).

The 3D map of structures shows that conformations 2902, 2903, 2907, 2909, and 2910 are similar among each other and different from other conformations (**Fig. 6A**). Also, in a very simplified form, it seems that the other conformations are projected so that they belong to two different groups that are similarly distant from the central group (2902, 2903, 2907, 2909, and 2910). One group comprises conformations 2904-2906, whereas the other group is made of conformations 2875, 2908, 2911 (**Fig. 6A**). The overlapped density maps (Fig. 7, together with Figs. S1 and S2 that are given in the Supporting Material) show that the three different coarse groups can be explained by the existence of at least two different types of changes in conformation and composition of the complex. One of them is a rotation of the small subunit (40S) with respect to the large subunit (60S), which could explain the group 2904-2906 (40S is rotated in these maps, with different amounts of rotation, as shown in panels L-O in **Fig. 7** and **Fig. S1**). The other is rolling of the complex, which could explain the central group of maps. Indeed, different degrees of rolling of the complex can be noticed in maps 2902, 2903, 2907, 2909, and 2910 (panels A-H in **Fig. 7** and **Fig. S1**). The remaining group is comprised of maps of complexes with slightly different degrees of unrolling and different compositions (2875, 2908, and 2911) (panels I-J in **Fig. 7** and **Fig. S1**). More precisely, in 2875, the A and F sites are empty; in 2908, they are occupied by A/T tRNA (A site) and eEF1A (F site); finally, in 2911, the F site is empty and the A site is occupied by A/T tRNA (**Fig. 7I-K**). Note here that we used a mask that suits the shape of 2875 to compute pseudo-atomic models,

implying that computations were done using density maps with partly removed additional mass from the A and F sites (panels A-E of **Fig. S2**). The contribution of masking in this case was, thus, not only in removing the background noise, but also in focusing the analysis onto the conformational changes (by minimizing compositional differences while preserving the associated conformational differences).

Although a combined conformational and compositional heterogeneity is a very difficult case, the proposed method showed very interesting results such as the observed grouping of density maps into three coarse but interpretable groups, in the same space of distances, as well as a closed trajectory formed by connecting points in the distance space following the original proposal (**Fig. 6**). Interestingly enough, the trajectory form could be described as 8-like, particularly in the 2D distance space (**Fig. 6B**).

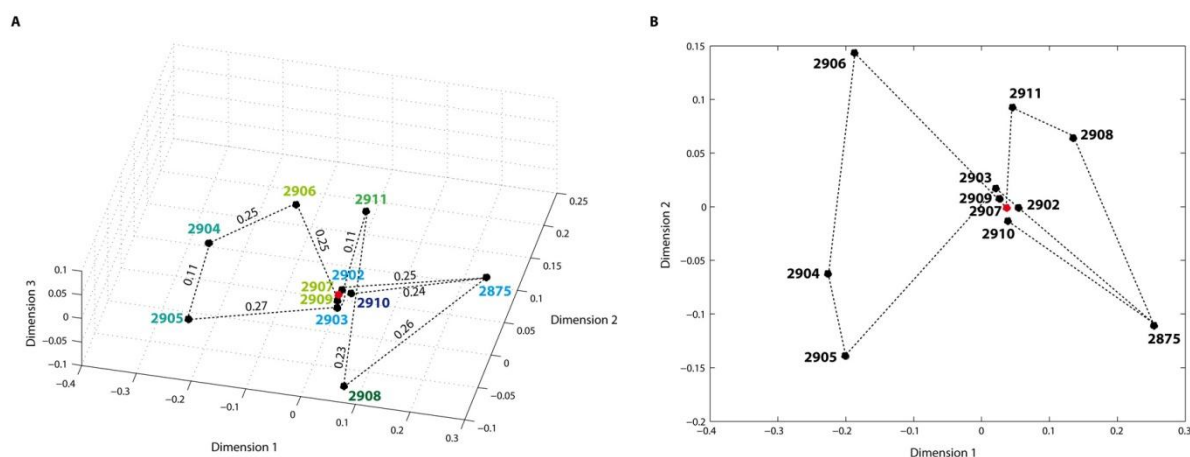


Figure 6: Projection of eleven EM density maps of 80S ribosome (EMD-2875 and from EMD-2902 to EMD-2911) onto 3D and 2D distance spaces. (A) 3D distance space. (B) 2D distance space. The density maps are marked with circles and the corresponding EMD entry codes. The length of each dotted line segment is the distance between two density maps that is, in A, shown above the segment in arbitrary units. The dotted lines are used to connect subsequent states according to the proposal by Behrmann et al (25). In A, different colors are used for map numbers to represent complexes with different compositions, according to Behrmann et al (25). The same colors are attributed to the maps with the same or similar composition, which resulted in the use of 6 different colors for the following types of composition: 1) 2904-2905 (two tRNAs but slightly different, P/E, A/P in 2905 and P/E, A/A in 2904); 2) 2906-2909 (three tRNAs: E/E, P/P, A/A); 3) 2902-2903 and 2875 (two tRNAs: E/E, P/P); 4) 2911 (three tRNAs: E/E, P/P, A/T); 5) 2908 (eEF1A and three tRNAs: E/E, P/P, A/T), 6) 2910 (eRF1, ABCE1, and two tRNAs: E/E,P/P). The classical iPRE state (EMD-2907) is marked with a red point in A-B. See also **Figure 7**.

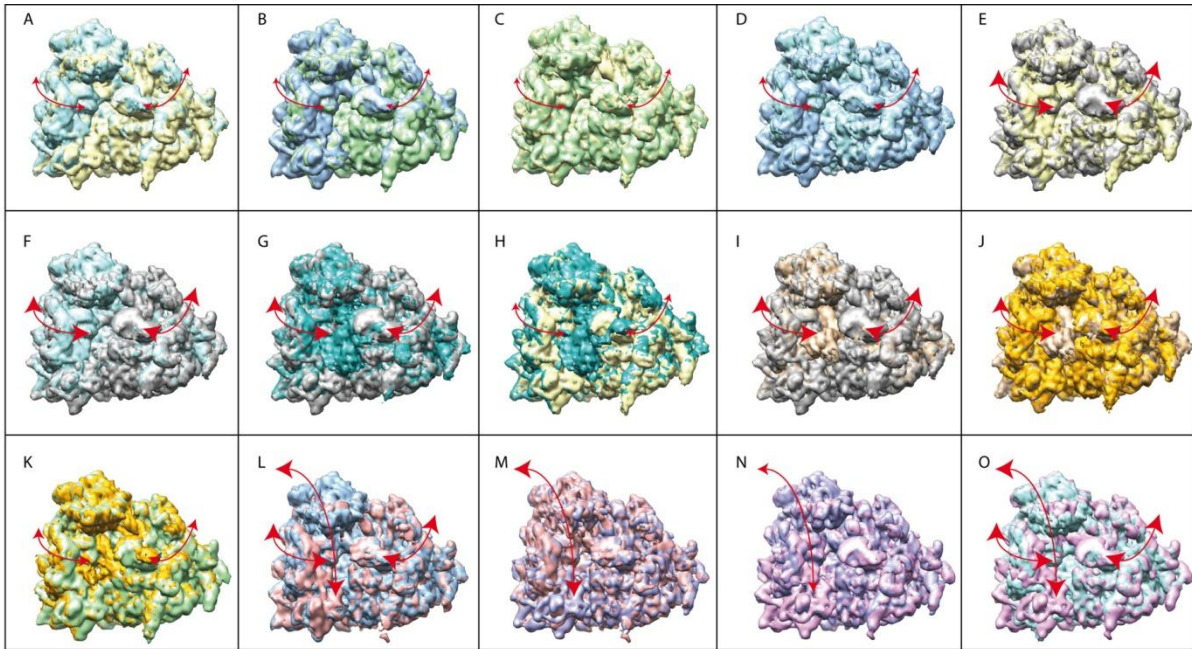


Figure 7: Overlap of rigid-body aligned EM density maps of 80S ribosome (EMD-2875 and from EMD-2902 to EMD-2911), with the same view for all overlapped density maps. (A) 2902 (yellow) vs 2903. (B) 2907 (green) vs 2909. (C) 2902 (yellow) vs 2907. (D) 2903 (cyan) vs 2909. (E) 2875 (grey) vs 2902. (F) 2875 (grey) vs 2903. (G) 2875 (grey) vs 2910. (H) 2902 (yellow) vs 2910. (I) 2875 (grey) vs 2908. (J) 2908 (brown) vs 2911. (K) 2911 (orange) vs 2907. (L) 2906 (pink) vs 2909. (M) 2906 (pink) vs 2904. (N) 2904 (blue) vs 2905. (O) 2905 (magenta) vs 2903. In each of panels A-O, arrows show the movements that mainly contribute to the elastic transformation (deformation) between two overlapped maps, and the arrow scale shows the distance between these maps in the distance space. Bi-directional arrows were used to recall that StructMap computes the elastic transformation between two maps in both directions. Note that the arrow scale shows dissimilarity between maps after the deformation but the amount of deformation (movement amount) is not represented by arrows. However, note that the type of movement is represented by arrows (i.e., rolling/unrolling of the complex in A-K, rotation of 40S with respect to 60S in M-N, and combination of rolling/unrolling and 40S rotation in L,O). See also **Figure 6** and **Figures S1 and S2**.

DISCUSSION AND CONCLUSION

In this paper, we presented StructMap that is, to the best of our knowledge, the first methodology allowing visualizing conformational differences among sets of EM density maps in a common and quantitative space while involving elastic alignment of these EM maps for conformational modeling. The elastic alignment of two EM maps is done by flexible deformation, using normal modes, of one map until it fits the other map. The elastic alignment allows building a matrix of distances among density maps, which is then analyzed to represent all density maps in the common distance space that is also referred to as “map of structures”.

StructMap does not impose any requirements regarding the mass of the complex or the size of its dynamic part. The only requirement is that all EM maps have the same size (number of voxels) and the same voxel size. Also, the work of StructMap will be facilitated if the complex is masked in the density maps to suppress the background noise. Masking of density maps is a part of common data processing workflows, and we expect that it will be done before starting StructMap. Otherwise, masking can be performed with the HEMNMA graphical interface. Masking can also be used to minimize the impact of compositional differences of complexes (e.g., due to ligand binding) onto the analysis of conformational differences among these complexes. The method works with EM maps that are usually available at different resolutions due to the use of different numbers of particles for their reconstruction and other experimental imaging related issues. In this article, we showed that

StructMap yields reliable results (in agreement with previously published results) for EM maps of different resolutions, more precisely, different resolution ranges (5-10 Å, 12-20 Å, 23-25 Å) of EM maps reconstructed from negative stain images (Pol α – B) or cryo images (70S and 80S). A higher resolution homogeneity of a set of EM maps is expected to yield a better resolution of conformational differences for the average level of details in that set of maps. Also, a higher resolution of all EM maps in the set is expected to yield a more precise analysis of smaller conformational changes.

Beyond discrete states

Results obtained with synthetic and experimental data show a great potential of the proposed method. Results obtained with experimental data of Pol α – B, 70S, and 80S complexes are fully consistent with previously published results. Moreover, the results presented here complement the previous results with a quantitative analysis of given density maps, which produces an original graphical representation of dissimilarities among the density maps.

The experiment with EM density maps of human 80S ribosomal complexes from polysomes shows a particularly challenging case of heterogeneity, which clearly demonstrates the usefulness of the proposed method. Indeed, the EM density maps used in that experiment represent 11 states of the ribosome during the elongation cycle and the EM maps differ among each other in both conformation and composition of the complex. With this data set, we observed a grouping of EM density maps in three coarse but interpretable groups and we obtained a closed trajectory by connecting the EM maps in the obtained distance space following the sequence proposed by the authors of the maps (25).

Possible trajectories of points in the map of structures

In some cases, trajectories of points can be inferred by connecting points in the map of structures, which suggests a possibility to explore potential sequences of conformational changes. The points can be connected in many different ways and, here, we would like to discuss possible *ad hoc* alternatives, or “rules”, to analyze the cloud of points, especially in the absence of *a priori* information about conformational changes of the studied complex. One of such rules could be to identify the shortest trajectory between two most extreme or distant points, taking into account the assumption that the shortest trajectory corresponds to the lowest “energy” or “effort” required to go from one extreme state to the other (e.g., states 3 and 5 on the 3-2-1-4-5 trajectory in Experiment 1 are the two most distant states and they correspond to maximally closed and maximally open synthetic symmetric conformations of the complex). Another possible rule is to identify the trajectory of points corresponding to those EM density maps that result from the largest numbers of single particle images, taking into account the assumption that a larger number of images used to reconstruct an EM map means a higher probability that the complex adopts this state. One could also think of combining such rules or even analyzing longer trajectories, taking into account possible random thermal motions of the complex in solution (9).

Network and graph analysis of conformational transitions has been also proposed in the context of analyzing protein conformational ensembles obtained by sampling the conformational space during molecular dynamics simulation of an atomic-resolution (X-ray or NMR) structure, the sampled conformations and transitions being considered as nodes and links of the network, respectively (38-40). The analysis of potential sequences of conformational changes is particularly difficult in the case of experimental EM maps and can additionally be hindered by a combined conformational and compositional heterogeneity of complexes, as observed in the experiment with the 80S ribosomal complex. Thus, though *ad*

hoc rules could help to start the analysis, additional information about the complex should be employed to ascertain the structural processes that actually take place. This is the reason why we did not use such rules in this article. We instead decided to complement the original work by analyzing similarities and dissimilarities among density maps based on their distances in the obtained distance space as well as by showing the pattern obtained after connecting the density maps in this distance space following the sequence proposed in the original publication.

Combination with “continuous” analysis of images

StructMap could be combined with techniques for “continuous” analysis of images, such as HEMNMA (8, 29), to explore continuous conformational changes more extensively. In this context, EM maps obtained by discretizing flexibility analysis would be analyzed by StructMap to better understand differences among maps and select a few of them for their use as the reference conformations for the “continuous” image analysis. HEMNMA, providing an overall view of the conformational distribution based on a 3D-to-2D elastic alignment of images with a given reference EM density map, would be used to perform a fine analysis of the dynamics around the reference conformations identified with the help of StructMap. This approach would be less computationally expensive than performing a fine analysis around every map from the given set of EM density maps. As StructMap performs an automatic analysis and projection of EM density maps onto a common distance space, it would be especially useful if the given set of density maps is large (e.g., containing more than 5 maps). Though the number of density maps obtained in the same experiment is typically smaller than 10, some studies result in much larger numbers of EM density maps (e.g., 50 maps were obtained in (15)). In the same context, StructMap could be combined with other approaches for exhaustive analysis of continuous conformational changes. For instance, StructMap could be used to select reference density maps to rigid-body align images before their analysis by the method proposed in (9).

The work presented in this article opens doors for further developments of such combined discrete-continuous approaches. To allow an easy and broad use of StructMap, this methodology is currently implemented in Scipion (<http://scipion.cnb.csic.es>).

SUPPORTING MATERIAL

Supporting Material includes three supplementary tables (Tables S1-S3) and two supplementary figures and their legends (**Figs. S1-S2**).

AUTHOR CONTRIBUTIONS

COSS and SJ designed the method and the experiments. COSS and MK implemented the method. COSS, SJ, and ALAC performed the experiments. COSS, SJ, ALAC and JMC discussed the results. SJ wrote the manuscript. JMC, COSS, ALAC, and MK reviewed the manuscript.

ACKNOWLEDGMENTS

The work was partially funded by the CNRS (France) and the CSIC (Spain) [Projet International de Coopération Scientifique - PICS 2011]; the French National Research Agency ANR [ANR-11-BSV8-010-04]; the European Social Fund and the Ministerio de Educación y Ciencia [“Ramón y Cajal” fellowship to COSS]; the Spanish Ministry of Economy and Competitiveness [AIC-A-2011-0638 and BIO2013-44647-R]; and the Comunidad de Madrid [CAM S2010/BMD-2305]. We thank GENCI-CINES/IDRIS (France) for HPC resources [x2013072174, x2014072174, x2015072174]; L. Pellegrini, S. Klinge

(Cambridge University, UK) and O. Llorca (CIB-CSIC, Spain) for generously providing the Pol α – B EM structures; and Dr Isabelle Callebaut (IMPMC, Paris, France) for stimulating discussions.

COMPETING FINANCIAL INTERESTS

The authors declare no competing financial interests.

REFERENCES

1. Frank, J. 1996. *Three-Dimensional Electron Microscopy of Macromolecular Assemblies*. Academic Press, San Diego.
2. Penczek, P. A., J. Frank, and C. M. Spahn. 2006. A method of focused classification, based on the bootstrap 3D variance analysis, and its application to EF-G-dependent translocation. *J Struct Biol* 154:184-194.
3. Scheres, S. H., H. Gao, M. Valle, G. T. Herman, P. P. Eggermont, J. Frank, and J. M. Carazo. 2007. Disentangling conformational states of macromolecules in 3D-EM through likelihood optimization. *Nat Methods* 4:27-29.
4. Fu, J., H. Gao, and J. Frank. 2007. Unsupervised classification of single particles by cluster tracking in multi-dimensional space. *J Struct Biol* 157:226-239.
5. Elad, N., D. K. Clare, H. R. Saibil, and E. V. Orlova. 2008. Detection and separation of heterogeneity in molecular complexes by statistical analysis of their two-dimensional projections. *J Struct Biol* 162:108-120.
6. Yang, Z., J. Fang, J. Chittuluru, F. J. Asturias, and P. A. Penczek. 2012. Iterative stable alignment and clustering of 2D transmission electron microscope images. *Structure* 20:237-247.
7. Lyumkis, D., A. F. Brilot, D. L. Theobald, and N. Grigorieff. 2013. Likelihood-based classification of cryo-EM images using FREALIGN. *J Struct Biol* 183:377-388.
8. Jin, Q., C. O. Sorzano, J. M. de la Rosa-Trevin, J. R. Bilbao-Castro, R. Nunez-Ramirez, O. Llorca, F. Tama, and S. Jonic. 2014. Iterative elastic 3D-to-2D alignment method using normal modes for studying structural dynamics of large macromolecular complexes. *Structure* 22:496-506.
9. Dashti, A., P. Schwander, R. Langlois, R. Fung, W. Li, A. Hosseinizadeh, H. Y. Liao, J. Pallesen, G. Sharma, V. A. Stupina, A. E. Simon, J. D. Dinman, J. Frank, and A. Ourmazd. 2014. Trajectories of the ribosome as a Brownian nanomachine. *Proc Natl Acad Sci U S A* 111:17492-17497.
10. Katsevich, E., A. Katsevich, and A. Singer. 2015. Covariance Matrix Estimation for the Cryo-EM Heterogeneity Problem. *SIAM J Imaging Sci* 8:126-185.
11. Tagare, H. D., A. Kucukelbir, F. J. Sigworth, H. Wang, and M. Rao. 2015. Directly reconstructing principal components of heterogeneous particles from cryo-EM images. *J Struct Biol* 191:245-262.
12. Grob, P., M. J. Cruse, C. Inouye, M. Peris, P. A. Penczek, R. Tjian, and E. Nogales. 2006. Cryo-Electron Microscopy Studies of Human TFIID: Conformational Breathing in the Integration of Gene Regulatory Cues. *Structure* 14:511-520.
13. Simonetti, A., S. Marzi, A. G. Myasnikov, A. Fabbretti, M. Yusupov, C. O. Gualerzi, and B. P. Klaholz. 2008. Structure of the 30S translation initiation complex. *Nature* 455:416-420.
14. Klinge, S., R. Nunez-Ramirez, O. Llorca, and L. Pellegrini. 2009. 3D architecture of DNA Pol alpha reveals the functional core of multi-subunit replicative polymerases. *Embo J* 28:1978-1987.
15. Fischer, N., A. L. Konevega, W. Wintermeyer, M. V. Rodnina, and H. Stark. 2010. Ribosome dynamics and tRNA movement by time-resolved electron cryomicroscopy. *Nature* 466:329-333.

16. Lyumkis, D., S. K. Doamekpor, M. H. Bengtson, J. W. Lee, T. B. Toro, M. D. Petroski, C. D. Lima, C. S. Potter, B. Carragher, and C. A. Joazeiro. 2013. Single-particle EM reveals extensive conformational variability of the Ltn1 E3 ligase. *Proc Natl Acad Sci U S A* 110:1702-1707.
17. van Heel, M., and J. Frank. 1981. Use of multivariate statistics in analysing the images of biological macromolecules. *Ultramicroscopy* 6:187-194
18. van Heel, M., and J. Frank. 1980. Classification of particles in noisy electron micrographs using correspondence analysis. In *Pattern Recognition in Practice I*. L. S. Gelsema, and L. Kanal, editors. North-Holland, Amsterdam. 235–243.
19. Suhre, K., J. Navaza, and Y. H. Sanejouand. 2006. NORMA: a tool for flexible fitting of high-resolution protein structures into low-resolution electron-microscopy-derived density maps. *Acta Crystallogr D Biol Crystallogr* 62:1098-1100.
20. Tama, F., O. Miyashita, and C. L. Brooks, 3rd. 2004. Flexible multi-scale fitting of atomic structures into low-resolution electron density maps with elastic network normal mode analysis. *J Mol Biol* 337:985-999.
21. Chacon, P., F. Tama, and W. Wrighers. 2003. Mega-Dalton biomolecular motion captured from electron microscopy reconstructions. *J Mol Biol* 326:485-492.
22. Tama, F., W. Wrighers, and C. L. Brooks, 3rd. 2002. Exploring global distortions of biological macromolecules and assemblies from low-resolution structural information and elastic network theory. *J Mol Biol* 321:297-305.
23. Ming, D., Y. Kong, M. A. Lambert, Z. Huang, and J. Ma. 2002. How to describe protein motion without amino acid sequence and atomic coordinates. *Proceedings of the National Academy of Sciences* 99:8620-8625.
24. Samsó, M., W. Feng, I. N. Pessah, and P. D. Allen. 2009. Coordinated movement of cytoplasmic and transmembrane domains of RyR1 upon gating. *PLoS Biol* 7:e85.
25. Behrmann, E., J. Loerke, T. V. Budkevich, K. Yamamoto, A. Schmidt, P. A. Penczek, M. R. Vos, J. Burger, T. Mielke, P. Scheerer, and C. M. Spahn. 2015. Structural snapshots of actively translating human ribosomes. *Cell* 161:845-857.
26. Chen, Y., S. Pfeffer, T. Hrabe, J. M. Schuller, and F. Forster. 2013. Fast and accurate reference-free alignment of subtomograms. *J Struct Biol* 182:235-245.
27. Nogales-Cadenas, R., S. Jonic, F. Tama, A. A. Arteni, D. Tabas-Madrid, M. Vazquez, A. Pascual-Montano, and C. O. Sorzano. 2013. 3DEM Loupe: Analysis of macromolecular dynamics using structures from electron microscopy. *Nucleic Acids Res* 41:W363-367.
28. Tirion, M. M. 1996. Large Amplitude Elastic Motions in Proteins from a Single-Parameter, Atomic Analysis. *Phys Rev Lett* 77:1905-1908.
29. Sorzano, C. O., J. M. de la Rosa-Trevin, F. Tama, and S. Jonic. 2014. Hybrid Electron Microscopy Normal Mode Analysis graphical interface and protocol. *J Struct Biol* 188:134-141.
30. Powell, M. J. D. 2002. UOBYQA: unconstrained optimization by quadratic approximation. *Mathematical Programming* 92:555-582.
31. Berghen, F. V., and H. Bersini. 2005. CONDOR, a new parallel, constrained extension of Powell's UOBYQA algorithm: Experimental results and comparison with the DFO algorithm. *J Comput Appl Math* 181:157-175.
32. Sorzano, C. O., R. Marabini, J. Velazquez-Muriel, J. R. Bilbao-Castro, S. H. Scheres, J. M. Carazo, and A. Pascual-Montano. 2004. XMIPP: a new generation of an open-source image processing package for electron microscopy. *J Struct Biol* 148:194-204.
33. Scheres, S. H., R. Nunez-Ramirez, C. O. Sorzano, J. M. Carazo, and R. Marabini. 2008. Image processing for electron microscopy single-particle analysis using XMIPP. *Nat Protoc* 3:977-990.
34. de la Rosa-Trevin, J. M., J. Oton, R. Marabini, A. Zaldivar, J. Vargas, J. M. Carazo, and C. O. Sorzano. 2013. Xmipp 3.0: an improved software suite for image processing in electron microscopy. *J Struct Biol* 184:321-328.

35. Cox, T. F., and M. A. A. Cox. 2001. *Multidimensional Scaling*. Chapman & Hall/CRC, Boca Raton, FL.
36. Velazquez-Muriel, J. A., C. O. Sorzano, J. J. Fernandez, and J. M. Carazo. 2003. A method for estimating the CTF in electron microscopy based on ARMA models and parameter adjustment. *Ultramicroscopy* 96:17-35.
37. Bruschiweiler, R. 1995. Collective protein dynamics and nuclear spin relaxation. *J Chem Phys* 102:3396–3403.
38. Ahlstrom, L. S., J. L. Baker, K. Ehrlich, Z. T. Campbell, S. Patel, Vorontsov, II, F. Tama, and O. Miyashita. 2013. Network visualization of conformational sampling during molecular dynamics simulation. *J Mol Graph Model* 46:140-149.
39. Morcos, F., S. Chatterjee, C. L. McClendon, P. R. Brenner, R. Lopez-Rendon, J. Zintsmaster, M. Ercsey-Ravasz, C. R. Sweet, M. P. Jacobson, J. W. Peng, and J. A. Izaguirre. 2010. Modeling conformational ensembles of slow functional motions in Pin1-WW. *PLoS Comput Biol* 6:e1001015.
40. Caflisch, A. 2006. Network and graph analyses of folding free energy surfaces. *Curr Opin Struct Biol* 16:71-78.

SUPPORTING MATERIAL TO:

StructMap: Elastic distance analysis of electron microscopy maps for studying conformational changes

C. O. S. Sorzano¹, A. L. Alvarez-Cabrera¹, M. Kazemi¹, J. M. Carazo¹, and S. Jonic^{2,*}

¹ Biocomputing Unit, Centro Nacional de Biotecnología – CSIC, Campus de Cantoblanco, Darwin 3,
28049 Madrid, Spain.

² IMPMC, Sorbonne Universités - CNRS UMR 7590, UPMC Univ Paris 6, MNHN, IRD UMR 206,
75005 Paris, France.

* Corresponding author (Slavica Jonic, IMPMC-UMR 7590, Université Pierre & Marie Curie, Case
courrier 115, 4 Place Jussieu, 75005 Paris, France, Phone : +33 1 44 27 72 05, Fax : +33 1 44 27 37
85, E-mail : Slavica.Jonic@impmc.upmc.fr).

SUPPLEMENTARY FIGURE LEGENDS:

Figure S1: Overlap of rigid-body aligned EM density maps of 80S ribosome (EMD-2875 and from EMD-2902 to EMD-2911), with the same view for all overlapped density maps but a different view with respect to **Figure 7**. (A) 2902 (yellow) vs 2903. (B) 2907 (green) vs 2909. (C) 2902 (yellow) vs 2907. (D) 2903 (cyan) vs 2909. (E) 2875 (grey) vs 2902. (F) 2875 (grey) vs 2903. (G) 2875 (grey) vs 2910. (H) 2902 (yellow) vs 2910. (I) 2875 (grey) vs 2908. (J) 2908 (brown) vs 2911. (K) 2911 (orange) vs 2907. (L) 2906 (pink) vs 2909. (M) 2906 (pink) vs 2904. (N) 2904 (blue) vs 2905. (O) 2905 (magenta) vs 2903. In each of panels A-O, arrows show the movements that mainly contribute to the elastic transformation (deformation) between two overlapped maps, and the arrow scale shows the distance between these maps in the distance space. Bi-directional arrows were used to recall that StructMap computes the elastic transformation between two maps in both directions. Note that the arrow scale shows dissimilarity between maps after the deformation but the amount of deformation (movement amount) is not represented by arrows. However, note that the type of movement is represented by arrows and it is the same as in **Figure 7** (i.e., rolling/unrolling of the complex in A-K, rotation of 40S with respect to 60S in M-N, and combination of rolling/unrolling and 40S rotation in L,O).

Figure S2: Overlap of rigid-body aligned EM density maps of 80S ribosome (EMD-2875 and from EMD-2902 to EMD-2911) as in **Figure 7G-K** (A-E, respectively) and panels G-K of **Figure S1** (F-J, respectively) but with EM density maps masked using a mask suited to the shape of EMD-2875. (A,F) 2875 (grey) vs 2910. (B,G) 2902 (yellow) vs 2910. (C,H) 2875 (grey) vs 2908. (D,I) 2908 (brown) vs 2911. (E,J) 2911 (orange) vs 2907. In each of panels A-J, arrows show the movements that mainly contribute to the elastic transformation (deformation) between two overlapped maps, and the arrow scale shows the distance between these maps in the distance space. Bi-directional arrows were used to recall that StructMap computes the elastic transformation between two maps in both directions. Note that the arrow scale shows dissimilarity between maps after the deformation but the amount of deformation (movement amount) is not represented by arrows. However, note that the type of movement is represented by arrows and it is the same for the top and bottom rows of a column because the column contains two views of the same pair of overlapped density maps. Finally, note that the pairs of maps shown in this figure present only rolling/unrolling movement of the complex.

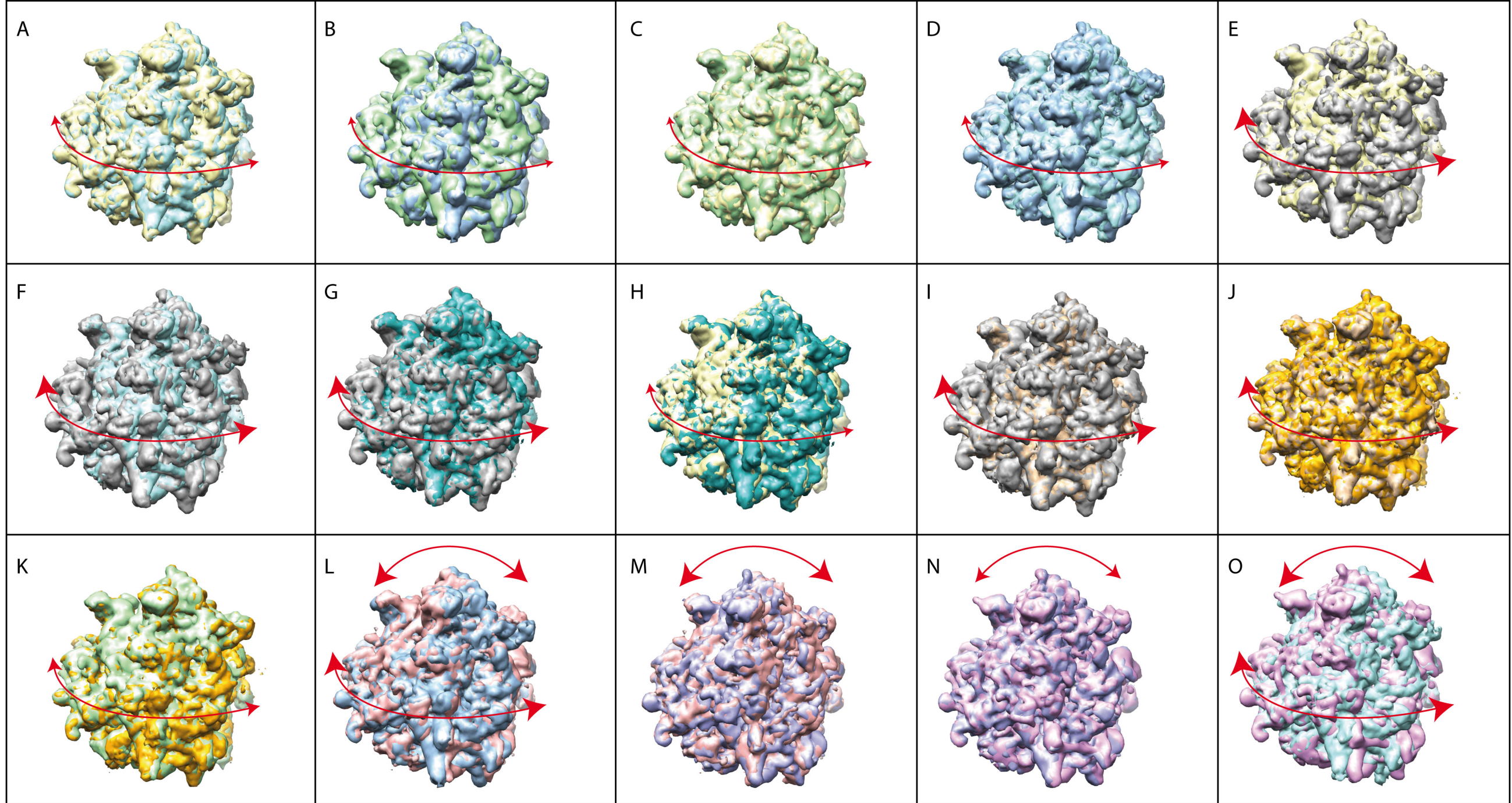


Figure S1

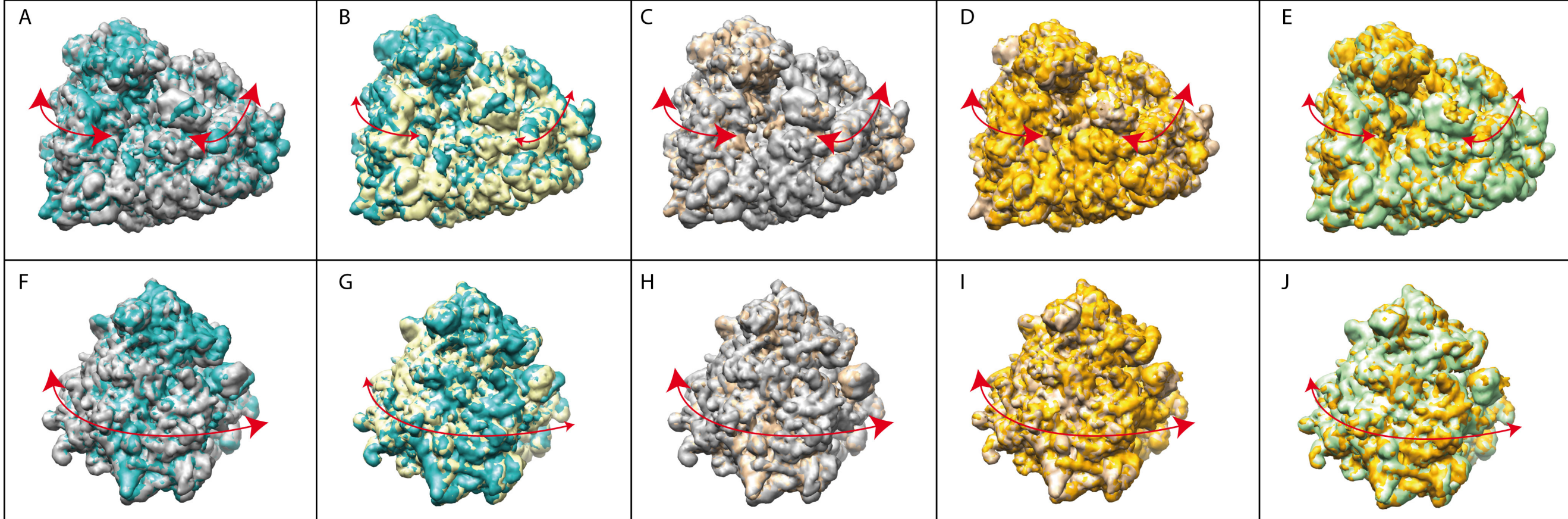


Figure S2

	1	2	3	4	5	6	7	8	9
1	0	0.03	0.06	0.03	0.06	0.04	0.07	0.04	0.06
2	0.03	0	0.03	0.07	0.09	0.06	0.07	0.06	0.07
3	0.06	0.03	0	0.09	0.12	0.08	0.09	0.07	0.08
4	0.03	0.07	0.09	0	0.03	0.06	0.07	0.06	0.07
5	0.06	0.09	0.12	0.03	0	0.07	0.09	0.07	0.09
6	0.04	0.06	0.08	0.06	0.07	0	0.06	0.08	0.11
7	0.07	0.07	0.09	0.07	0.09	0.06	0	0.11	0.13
8	0.04	0.06	0.07	0.06	0.07	0.08	0.11	0	0.03
9	0.06	0.07	0.08	0.07	0.09	0.11	0.13	0.03	0

Table S1: Pairwise distances (in arbitrary units) among synthetic RyR1 density maps 1-9 projected onto the 3D distance space shown in **Fig. 2F**.

	1717	1718	1719	1720	1721	1722	1723
1717	0	0.11	0.20	0.21	0.20	0.25	0.25
1718	0.11	0	0.11	0.11	0.20	0.20	0.30
1719	0.20	0.11	0	0.11	0.30	0.25	0.35
1720	0.21	0.11	0.11	0	0.30	0.30	0.40
1721	0.20	0.20	0.30	0.30	0	0.13	0.25
1722	0.25	0.20	0.25	0.30	0.13	0	0.25
1723	0.25	0.30	0.35	0.40	0.25	0.25	0

Table S2: Pairwise distances (in arbitrary units) among seven EM density maps of 70S ribosome (EMD-1717 to EMD-1723) projected onto the 3D distance space shown in **Fig. 5A**.

	2875	2902	2903	2904	2905	2906	2907	2908	2909	2910	2911
2875	0	0.25	0.25	0.49	0.51	0.44	0.25	0.26	0.25	0.24	0.24
2902	0.25	0	0.04	0.25	0.26	0.25	0.01	0.13	0.01	0.04	0.10
2903	0.25	0.04	0	0.26	0.27	0.29	0.04	0.12	0.04	0.08	0.12
2904	0.49	0.25	0.26	0	0.11	0.25	0.25	0.33	0.25	0.27	0.26
2905	0.51	0.26	0.27	0.11	0	0.24	0.26	0.30	0.25	0.27	0.31
2906	0.44	0.25	0.29	0.25	0.24	0	0.25	0.32	0.25	0.23	0.27
2907	0.25	0.01	0.04	0.25	0.26	0.25	0	0.12	0.01	0.04	0.11
2908	0.26	0.13	0.12	0.33	0.30	0.32	0.12	0	0.12	0.12	0.23
2909	0.25	0.01	0.04	0.25	0.25	0.25	0.01	0.12	0	0.04	0.12
2910	0.24	0.04	0.08	0.27	0.27	0.23	0.04	0.12	0.04	0	0.13
2911	0.24	0.10	0.12	0.26	0.31	0.27	0.11	0.23	0.12	0.13	0

Table S3: Pairwise distances (in arbitrary units) among eleven EM density maps of 80S ribosome (EMD-2875 and from EMD-2902 to EMD-2911) projected onto the 3D distance space shown in **Fig. 6A**.